The developmentally-timed decay of an essential microRNA family is seed sequence-dependent

Bridget Donnelly[1,2], Bing Yang[1], Chen-Yu Liu[1], Katherine McJunkin[1,3]

[1]Laboratory of Cellular and Developmental Biology, NIDDK Intramural Research Program, 50 South Drive, Bethesda, MD, 20815, USA
[2]Johns Hopkins University Department of Biology, 3400 N. Charles Street, Baltimore, MD, 21218, USA
[3]Correspondence: mcjunkin@nih.gov

Abstract

MicroRNA (miRNA) abundance is tightly controlled by regulation of biogenesis and decay. Here we show that the *mir-35* miRNA family undergoes regulated decay at the transition from embryonic to larval development in *C. elegans*. The seed sequence of the miRNA is necessary and sufficient for this regulation. Sequences outside the seed (3' end) regulate *mir-35* abundance in the embryo but are not necessary for sharp decay at the transition to larval development. Enzymatic modifications of the miRNA 3' end are neither prevalent nor correlated with changes in decay, suggesting that miRNA 3' end display is not a core feature of this mechanism and further supporting a seed-driven decay model. Our findings demonstrate that seed sequence-specific decay can selectively and coherently regulate all redundant members of a miRNA seed family, a class of mechanism that has great biological and therapeutic potential for dynamic regulation of a miRNA family's target repertoire.

Introduction

microRNAs (miRNAs) are small non-coding RNAs (~22-23 nucleotides) that, when bound by Argonaute, form the miRNA-induced silencing complex (miRISC) and negatively regulate target mRNAs (Dallaire et al., 2018). The biogenesis of miRNAs has been well described; first, miRNAs are transcribed as a primary miRNA (pri-miRNA): a long transcript containing a ~35 base pair stem-loop structure formed by intramolecular base-pairing (Fang and Bartel, 2015; Han et al., 2006; Ma et al., 2013; Zeng et al., 2005). The double-stranded RNA hairpin structure of the pri-miRNA is recognized by the Microprocessor complex (Drosha and DGCR8/Pasha) (Fang and Bartel, 2015; Han et al., 2006; Ma et al., 2013; Zeng et al., 2005). The catalytic RNase III domain of Drosha cleaves the pri-miRNA, resulting in the generation of a miRNA precursor (pre-miRNA) hairpin structure with a two-nucleotide overhang at the 3' end (Denli et al., 2004; Gregory et al.,

2004; Han et al., 2004; Landthaler et al., 2004). Once exported from the nucleus, the pre-miRNA is cleaved by the RNase III enzyme Dicer into a ~22-23 nucleotide duplex that is loaded into Argonaute (Bernstein et al., 2001; Grishok et al., 2001; Hutvágner et al., 2001; Ketting et al., 2001; Knight and Bass, 2001). The mature guide strand remains in the Argonaute protein, becoming a part of the miRISC, while the star strand is ejected and degraded (Iwasaki et al., 2010, 2015). Once the mature miRNA is incorporated into miRISC, miRISC uses the bound miRNA guide strand to target complementary regions in the 3'UTR of mRNAs to silence gene expression by translational repression, deadenylation and decay of the target mRNA (Dexheimer and Cochella, 2020).

The interaction between the miRNA and mRNA target is primarily mediated through nucleotides 2-8 at the 5' end of the miRNA (Brennecke et al., 2005; Lewis et al., 2003). This region, called the seed sequence, is the defining characteristic of a miRNA family, a group of miRNAs that act largely redundantly on an overlapping set of target genes due to their identical seed sequences (Alvarez-Saavedra and Horvitz, 2010; Parchem et al., 2015). Additional supplemental base pairing between the 3' end of the miRNA and the target RNA occurs in some cases, conferring some differences in target repertoire of miRNA family members (which share a seed sequence but may differ in their 3' sequences) (Broughton et al., 2016; Brancati and Grosshans, 2018; Helwak et al., 2013; Ye Duan, Isana Veksler-Lublinsky, 2021).

While much is known about the biogenesis and functions of miRNAs, relatively little is known about the mechanisms of decay of mature miRNAs. While half-lives of miRNAs vary, what determines these differences in stability is for the most part unknown (Bail et al., 2010; Kingston and Bartel, 2019; Lehrbach et al., 2012; Marzi et al., 2016; Miki et al., 2014; Reichholf et al., 2019; Vieux et al., 2021). Thus far, multiple phenomena regulating miRNA stability have been observed, with different degrees of sequence-specificity.

Some decay pathways appear to be largely independent of miRNA sequence. In *C. elegans*, the 5' to 3' nuclease XRN-2, along with DCS-1, maintain wild type miRNA levels by degrading many (though not all) miRNAs (Bossé et al., 2013; Chatterjee et al., 2009). In the mouse retina, an undefined mechanism induces decay of most miRNAs upon light-dependent neuronal activity (Krol et al., 2010). At the maternal to zygotic transition in *Drosophila,* terminal adenylation of maternal miRNAs by the noncanonical poly(A) polymerase, Wispy, induces their wholesale clearance (Lee et al., 2014). In other species, 3' nucleotide addition (tailing) has also been proposed to destabilize miRNAs in a sequence-independent manner (Boele et al., 2014;

Katoh et al., 2015; Knouf et al., 2013; Lee et al., 2019; Shukla et al., 2019; Wyman et al., 2011; Yang et al., 2020a).

Other miRNA decay pathways are guided by moderate sequence-specificity. One example is Tudor SN-mediated miRNA decay (TumiD) (Elbarbary et al., 2017a, 2017b). In TumiD, the endonuclease Tudor-SN (TSN) cleaves a few dozen miRNAs at CA and UA dinucleotides greater than 5 nucleotides away from the 3' and 5' ends of the miRNA (Elbarbary et al., 2017a, 2017b). A more specific phenomenon confers instability to several members of the extended miR-16 family; this decay is dependent on sequences in the both the seed and the 3' portion of the miRNA (Rissland et al., 2011). Rapid decay of miR-382 is dependent on the 7 nucleotides at the 3' end of the miRNA (Bail et al., 2010).

The most sequence-specific mechanism of miRNA decay is called target-directed miRNA degradation (TDMD). TDMD occurs when a high-abundance RNA (the TDMD "trigger") binds to a miRNA with extensive complementarity to both the seed sequence and the 3' half of the miRNA (Ameres et al., 2010; Baccarini et al., 2011; Bitetti et al., 2018; Cazalla et al., 2010; Ghini et al., 2018; Kleaveland et al., 2018; Libri et al., 2012; Marcinowski et al., 2012; la Mata et al., 2015; Piwecka et al., 2017). This extensive base pairing induces a conformational change that pulls the 3' end of the miRNA out of the PAZ domain of Argonaute, making it accessible to modification by untemplated nucleotide additions (tailing) and exonucleolytic cleavage (trimming) (Sheu-Gruttadauria et al., 2019; Yang et al., 2020a). Recently, the Cullin-RING E3 ubiquitin ligase ZSWIM8 was identified as an effector of TDMD, leading to the model that the Argonaute conformation induced by extensive base pairing is recognized by ZSWIM8 for ubiquitylation and subsequent decay of the miRNA:Argonaute complex (Han et al., 2020; Shi et al., 2020).

The regulation of miRNA expression during development is crucial to ensure properly timed developmental transitions, but the extent to which miRNA decay contributes to ensuring proper temporal expression patterns of miRNAs and how development is coupled to regulated decay are not known.

In this work, we set out the examine the mechanism of decay of the *mir-35* family of miRNAs. The *mir-35* family consists of 8 miRNAs, *mir-35-42* (Alvarez-Saavedra and Horvitz, 2010). The *mir-35* family members are maternally contributed as well as zygotically expressed in early embryogenesis, and they are sharply degraded at the transition from embryo to the first larval stage, L1 (Stoeckius et al., 2009; Wu et al., 2010). Understanding the mechanism of this decay will shed light on how selective miRNA decay occurs and how it is coupled to development.

100 The *mir-35* family is one of two miRNA seed families that are necessary for *C. elegans* embryogenesis. Because of their identical seed sequences, the *mir-35* family members are functionally redundant; deletion of any single miRNA has no phenotypic consequences, whereas deletion of the whole family results in embryonic lethality (Alvarez-Saavedra and Horvitz, 2010). The *mir-35* family miRNAs also play multiple roles in development, including promoting maximal
105 fecundity, ensuring sex determination, and regulating cell death (Doll et al., 2019; Kagias and Pocock, 2015; Liu et al., 2011; Massirer et al., 2012; McJunkin and Ambros, 2014, 2017; Sherrard et al., 2017; Tran et al., 2019; Yang et al., 2020b; Zhao et al., 2019).

How the *mir-35* family is targeted for selective decay at the end of embryogenesis is not known. A recent study showed that the TDMD factor ZSWIM8 (known as EBAX-1 in *C. elegans*)
110 drives instability of the *mir-35* family, suggesting that the *mir-35* family is subject to TDMD (Shi et al., 2020; Wang et al., 2013). However, positions of the miRNA that are usually involved in the base-pairing interactions that drive TDMD (in the 3' half of the miRNA) are highly degenerate across the *mir-35* family members (Figure 1A), suggesting that the mechanism of *mir-35* decay may differ from previously-described examples of TDMD, and may represent a novel type of
115 selective miRNA decay mechanism.

Here we show that the *mir-35* family is regulated at the level of decay at the embryo to L1 transition in *C. elegans*. We demonstrate that the seed sequence of *mir-35* is necessary and largely sufficient for this developmentally timed decay. This decay is not correlated with high levels of miRNA 3' tailing and trimming. Together, these data suggest that this miRNA family is regulated
120 by a distinct – but possibly related – mechanism to TDMD. Seed-specific decay mechanisms such as this are likely to be more widespread in biological systems since they have potential to co-regulate all members of a redundant miRNA family, potentially allowing dynamic derepression of the miRNA family's target genes.

125 Results

mir-35 decay is seed sequence-dependent

The *mir-35* family is selectively decayed at the embryo to L1 transition (Stoeckius et al., 2009; Wu et al., 2010). We wondered if its decay is a regulated process or, alternatively, just a result of transcriptional shutoff in late embryogenesis. We also wondered whether its
130 characteristic seed sequence played a role in this putative regulated decay. To this end, we used CRISPR/Cas9 to mutate the genomic locus which encodes seven of the eight *mir-35* family

members, *mir-35-41,* on a single transcript (Figure 1B). (*mir-42* is clustered with unrelated miRNAs at a different genomic locus.) We made targeted mutations to the seed sequence of the first hairpin in the *mir-35-41* cluster (*mir-35*) using CRISPR/Cas9. This approach leaves the remainder of the *mir-35-41* cluster intact, which serves two purposes: 1) *mir-35* loss-of-function phenotypes are not induced since the other family members remain wild type, and 2) *mir-36-41* serve as internal controls derived from the same transcript as *mir-35*. Both strands of the hairpin encoding *mir-35* were mutated to preserve secondary structure and support efficient processing (Figure 1B). One of the mutations was a reversal of the seed sequence, referred to hereafter as *mir-35(seed_rev)*), whereas the other mutation replaced the *mir-35* seed sequence with random nucleotides (*mir-35(seed_mut)*) (Figure 1B).

To determine if biogenesis of *mir-35* was affected by these seed mutations, we quantified *mir-35* and the mutant variants using miRNA-Taqman qPCR, along with synthetic RNAs oligonucleotides to generate standard curves for absolute quantification (Figure S1). The embryo concentration of *mir-35(seed_ rev)* is similar to wild type *mir-35* (0.7-fold change), while *mir-35(seed_mut)* is ten-fold lower (Figure 1C). To determine if the changes in the level of the *mir-35* variants was at the level of biogenesis or post-biogenesis, we examined the abundance of their star strands in the embryo. Changes is abundance of the *mir-35* variant star strands is similar to those in the respective guide strands (Figure 1D); these coupled changes suggest that the decreased abundance of *mir-35(seed_mut)* is due to loss of efficiency in biogenesis.

Next, we examined whether the decay of *mir-35* at the embryo to L1 transition is altered by seed mutations. (Note that, because we use arrested L1 samples, post-embryogenesis growth has not begun, so any decreases in miRNA abundance must be attributed to decay rather than dilution caused by growth.) As expected, we observed a strong reduction in wild type *mir-35* at the transition from embryo to L1, with 12-fold lower abundance in L1 (Figure 1C). However, the decay of mutant *mir-35*(*seed_rev*) and *mir-35*(*seed_mut*) at the transition from embryo to L1 was greatly attenuated to essentially no change and 1.3-fold lower in L1 than embryo, respectively (Figure 1C). *mir-35(seed_rev)* derived from a second CRISPR allele with altered precursor secondary structure also showed attenuated decay (Figure S2). Therefore, the decay of *mir*-35 depends on its seed sequence. Importantly, the decay of *mir-36* was not altered by the mutations in *mir-35* (Figure 1C). This decoupling of the behavior of *mir-35* and *mir-36* – which share a primary transcript – further shows that *mir-35* decay is regulated post-transcriptionally.

To confirm and extend these findings, we performed deep sequencing to profile all miRNAs. Deep sequencing confirmed that *mir-35* was the only miRNA altered in abundance by

165 these mutations in embryo or L1 samples (Figure S3). Consistent with the qPCR, wild type *mir-35* displayed sharp decay at the embryo to L1 transition, and the *mir-35* seed mutants were resistant to this decay (Figure 1E). The decay of the other members of the *mir-35* family was not affected by *mir-35* seed mutations, despite most members sharing the *mir-35-41* primary transcript (Figure 1E). Global analysis further demonstrated the selectivity of the decay of the *mir-*
170 *35* family in this developmental window: *mir-35-41* represent seven of the eight most sharply downregulated miRNAs in this time point in wild type (Figure 1F). This analysis also reiterates the specificity of the effect of the *mir-35* seed mutations, further demonstrating that the regulation of other miRNAs is not affected by these mutations (Figure 1F).

Together these results show that the decay of the *mir-35* family at this developmental
175 transition is a regulated decay process (rather than the result of synchronous decay after transcriptional shutoff), since the behavior of miRNAs derived from the same transcript can be de-coupled. Furthermore, these results show that that the *mir-35* seed sequence is required for this regulated decay.

180 ***mir-35* 3' end mutants undergo efficient decay at the embryo to L1 transition**

The necessity of the seed sequence for *mir-35* decay (Figure 1) and the recent implication of the TDMD factor ZSWIM8/EBAX-1 in regulating stability of the *mir-35* family (Shi et al., 2020) together suggest a TDMD-like decay mechanism. However, the degeneracy of sequences in the 3' region of the miRNA across the *mir-35* family members (Figure 1A) suggests that the
185 mechanism may differ from previous examples of TDMD since multiple trigger RNAs would be necessary to bind with extensive complementarity to all the family members. (Note that results from *mir-35(seed_rev)* and *mir-35(seed_mut)* rule out an antisense RNA from the *mir-35-41* cluster acting as a TDMD trigger RNA, since mutations at the genomic locus would not disrupt base-pairing with an antisense transcript.)

190 Therefore, we next investigated whether the 3' portion of the miRNA plays a role in *mir-35* family decay and if the *mir-35* seed sequence is sufficient for decay. To test this, we used CRISPR to generate two *mir-35* mutant strains in which the non-seed (3' end) residues of the miRNA are mutated. The first mutant is comprised of the *mir-35* seed sequence with a 3' end containing nucleotides that are either not present or rare among all *mir-35* family members at a given
195 position, while preserving overall GC content (*mir-35(mut_3')*) (Figure 2A). The second mutant is a *mir-35/mir-82* hybrid composed of the *mir-35* seed sequence and *mir-82* 3' end (*mir-35(mir-*

82_3')) (Figure 2A). The *mir-82* sequence was chosen for the non-seed region of *mir-35* because *mir-82* expression is steady rather than downregulated at the embryo to L1 transition (Kato et al., 2009).

200 Again, we performed miRNA-Taqman qPCR of *mir-35* and its mutant variants, using synthetic miRNAs of known concentrations to generate standard curves for absolute quantification (Figure S1). In embryos, the quantity of *mir-35(mut_3')* and *mir-35(mir-82_3')* were increased 20-fold and 139-fold relative to wild type *mir-35*, respectively (Figure 2B). To determine whether these changes in abundance arise during or after biogenesis, we also performed
205 absolute quantification of the star strands of the *mir-35* variants. This analysis showed that the star strand abundances did not mirror changes in the guide strand abundances, suggesting that the large changes in guide strand abundance are post-biogenesis level effects, such as at the level of decay (Figure 2C). We therefore postulate that a second decay mechanism may act to limit abundance of *mir-35* in the embryo in a manner dependent upon the 3' end sequence (Figure
210 S4).

We next measured the decay of the *mir-35* 3' end variants at the embryo to L1 transition. Unlike the seed mutants, the change in the abundance of the *mir-35* 3' end mutants from the embryo to L1 stage was similar to that of wild type *mir-35* [7-fold for the *mir-35(mut_3')*, 14-fold for *mir-35(mir-82_3')*, and 8-fold for wild type] (Figure 2B). Likewise *mir-36* was not affected by
215 the mutations (Figure 2B). Again, we confirmed and extended these findings using deep sequencing. Deep sequencing confirmed that the 3' end variants showed a similar depletion from embryo to L1 stage as wild type *mir-35*, and that no other miRNAs in the *mir-35* family or otherwise were affected (Figure 2D-E, Figure S5). Thus, the sequence of the 3' end of the miRNA outside the seed did not affect the decay at this developmental transition.

220 Overall, we observed that seed mutations do not generally impact embryonic *mir-35* abundance but strongly inhibit its decay at the embryo to L1 transition, whereas 3' end mutations strongly impact embryonic abundance of *mir-35* but do not affect its decay at the embryo to L1 transition. Taken together, we propose that two decay mechanisms regulate *mir-35* abundance: a 3' end-dependent mechanism limits abundance in embryos, while a seed-dependent
225 mechanism drives decay at the transition to L1 (Figure S4). Given that all positions 3' of the seed sequence are mutated in the 3' end mutants, the seed sequence of *mir-35* is not only necessary but also largely sufficient to drive its regulated decay at the embryo to L1 transition.

mir-35 variants are tailed and trimmed similarly to wild type *mir-35*

230 While the seed-dependence and ZSWIM8/EBAX-1-dependence of *mir-35* regulation suggest a TDMD-like mechanism, the dispensability of the 3' end for developmentally timed turnover suggests an alternative mechanism. Another hallmark of TDMD is a high prevalence of tailing and trimming during the decay process, which is thought to be due to conformational changes induced by extensive base pairing, that expose the 3' end of the miRNA to exonucleases
235 and nucleotidyltransferases.

To determine whether the *mir-35* family bears this hallmark of TDMD, we examined the prevalence of tailing and trimming. We first examined the level of background in tailing measurements in our experimental and computational pipeline. To this end, synthetic miRNAs were spiked into total RNA after purification, and the amount of tailing called on these miRNAs is
240 considered background since these miRNAs were never present in the context of cellular lysate, so any apparent "tailing" must derive from errors introduced in cloning or sequencing. Tailing was below 1.5% in 317 out of 324 (98%) such spike-in measurements, so tailing below 1.5% is considered background in these datasets. This threshold is marked by a dashed line on all tailing plots.

245 In embryos and L1s, we observed that miRNAs are tailed to various extents, though generally not very high levels (Figure 3A, Figure S6A). Tailing was mostly mono-uridylation, with some miRNAs displaying significant adenylation or cytidylation, as previously observed (Figure 3A, Figure S6A) (Vieux et al., 2021). Overall tailing and miRNA abundance were not correlated, and the *mir-35* family members were generally high in abundance, with a wide range of tailing
250 frequencies observed across different members (Figure 3B).

We and others previously observed slight increases in the prevalence of tailed and trimmed miRNAs as miRNAs approach decay (Baccarini et al., 2011; Kingston and Bartel, 2019; Vieux et al., 2021). In TDMD, miRNAs experience very high levels of tailing and/or trimming (generally ≥20-40% tailed or trimmed isoforms) (Ameres et al., 2010; Baccarini et al., 2011; Bitetti
255 et al., 2018; Cazalla et al., 2010; Ghini et al., 2018; Kleaveland et al., 2018; Marcinowski et al., 2012). We hypothesized that the prevalence of tailed isoforms might increase at the embryo to L1 transition as the *mir-35* family members undergo decay. Small increases in miRNA tailing and trimming were observed, but in most cases, these were not statistically significant, and the prevalence of modified isoforms remained modest (Figure 3C, 3E).

260 We next examined the prevalence of tailed isoforms in the context of mutant versions of *mir-35*. Significant changes in tailing were observed, but interestingly, these did not correlate with changes in rates of decay (Figure 3D). For instance, *mir-35(mut_3')* was significantly more cytidylated and uridylated than wild type *mir-35* in embryo and L1, and *mir-35(mir-82_3')* was significantly more adenylated, cytidylated, and uridylated than wild type *mir-35* in both stages (p-
265 value < 0.05 for all aforementioned comparisons) (Figure 3D). However, these two *mir-35* variants displayed decay similar to that of wild type *mir-35* at the embryo to L1 transition (Figure 2B). In contrast, *mir-35(seed_rev)* and *mir-35(seed_mut)* show similar amounts of tailing to the wild type *mir-35* (Figure 3D), despite these variants' dramatically altered decay at the embryo to L1 transition (Figure 1C). Thus, changes in tailing did not correlate with changes in decay.

270 We next examined trimming of *mir-35* variants. Like tailing, trimming varied widely among *mir-35* variants, but not in a manner that correlated with the rate of decay. For instance, trimming increased most for *mir-35(seed_mut)*, despite the enhanced stability of this variant (Figure 3F, Figure S6B). In contrast, *mir-35(seed_rev)* – which shows similarly enhanced stability – had no significant change in trimming (Figure 3F, Figure S6B). This isoform analysis also showed that
275 *mir-35(mut_3')* yields two major isoforms from biogenesis, the canonical 22-nt isoform and a 23-nt isoform which is extended by 1nt at the 3' end (Figure 3F, Figure S6B). Analysis of deep sequencing data showed that both isoforms are decayed similarly at the embryo to L1 transition (Figure S7). Overall, changes in trimming did not correlate with changes in decay.

All together, these data show that the tailing and trimming of the *mir-35* family are much
280 lower in prevalence than in known instances of TDMD, and that the incidence of trimmed and tailed isoforms across *mir-35* variants did not correlate with rate of decay at the embryo to L1 transition. Together with the dispensability of the 3' end sequences of *mir-35* for decay, this suggests that the mechanism of decay of *mir-35* differs from previously described examples of TDMD.

285

Reintroducing miRNA-target interactions does not restore decay of seed mutant variants of *mir-35*

To further investigate the mechanism of *mir-35* family decay at the embryo to L1 transition,
290 we examined the possible involvement of complementary RNA molecules as in TDMD. Decay of *mir-35* at the embryo to L1 transition is dependent on its seed sequence but not its 3' end sequences, and canonical targets were previously shown to regulate miRNA stability in *C.*

elegans (Chatterjee et al., 2011). We therefore wondered whether canonical miRNA:target interactions (rather than TDMD-like base-pairing) might play a role in mediating this decay. To test this hypothesis, we restored canonical target interactions for a seed mutant variant of *mir-35* to determine whether this restored developmentally-timed decay.

To this end, we sought to alter a similar stoichiometric proportion of the pool of *mir-35* family miRNAs and the pool of *mir-35* family targets. *mir-35* makes up 20% of the *mir-35-42* miRNA molecules in embryos based on quantitative deep sequencing (Dexheimer et al., 2020), so we selected three target genes that together also make up 20% of the target molecules (as estimated from embryo RNAseq datasets) (Grün et al., 2014). These genes – *egl-1, nhl-2,* and *sup-26* – were also selected because they are all validated targets that influence physiology downstream of *mir-35-42* (Kagias and Pocock, 2015; McJunkin and Ambros, 2017; Sherrard et al., 2017; Tran et al., 2019; Wu et al., 2010; Yang et al., 2020b). Using CRISPR, we made mutations to the *mir-35* family binding site in the 3'UTR of these three target genes. These mutations enable binding by *mir-35(seed_rev)* rather than wild type *mir-35*, and we have previously shown that *mir-35(seed_rev)* represses such targets (Figure 4A) (Yang et al., 2020b).

We performed qPCR to measure the miRNA levels in the embryo and L1 stages. Again, we observed a significant reduction in wild type *mir-35* from embryo to L1 and attenuated decay of the *mir-35(seed_rev)* (Figure 4B). Wild type *mir-35* decay was not affected by the mutations of the target sites (Figure 4B). When *mir-35(seed_rev)* was combined with the mutant targets containing complementary binding sites, decay was similar to *mir-35(seed_rev)* without engineered target interactions (Figure 4B). Thus, restoring interactions with canonical target genes is not sufficient to restore turnover of the *mir-35* seed mutant.

Discussion

Here we investigate the regulation of the embryonically-expressed *mir-35* family during development. We show that the decay of these miRNAs at the embryo to L1 transition is regulated post-transcriptionally, since mutations in the seed sequence of *mir-35* decouple its regulation from that of its clustermates on the same transcript, strongly supporting a regulated decay mechanism.

The seed sequence of *mir-35* is not only necessary for this regulated decay, but is also sufficient since mutations in the 3' end of the miRNA do not disrupt decay at the embryo to L1 transition. We do observe, however, that the 3' end regulates *mir-35* abundance in the embryo, in what appears to be a decay-level effect. We postulate that, whereas a seed-dependent decay

mechanism enacts developmentally-timed decay, a 3' end-dependent mechanism limits *mir-35* abundance in the embryo (Figure S4).

While the TDMD factor ZSWIM8/EBAX-1 regulates *mir-35* abundance, our data argues that the mechanisms of *mir-35* regulation differ from TDMD in key aspects (Figure 4C-E). First, the decay at embryo to L1 does not require the 3' end sequences which would be involved in base pairing to a typical TDMD trigger RNA. Second, the decay is not accompanied by high levels of tailing or trimming. Furthermore, seed mutations that reduce decay do not reduce tailing or trimming. Together, these data suggest that the *mir-35* family is post-transcriptionally regulated by a novel seed-dependent mechanism. We further observed that the altered regulation of seed mutants was not due to loss of target interactions, since restoring these interactions did not restore decay.

We propose a model for *mir-35* family decay wherein ZSWIM8/EBAX-1 is recruited to degrade the miRISC in a seed-dependent manner that does not require extensive 3' end base pairing. How the seed is recognized and how ZSWIM8/EBAX-1 is recruited in this process will be an area of ongoing study. Like TDMD, a trigger RNA may base pair with the *mir-35* family seed sequence and recruit an RNA binding protein, which can in turn recruit ZSWIM8/EBAX-1 (Figure 4D). Alternatively, the trigger RNA could induce conformational changes in Argonaute that directly recruit ZSWIM8/EBAX-1, similar to proposed models of TDMD. A third possibility is that no trigger RNA is involved in seed recognition for decay; in this case an RBP could bind the *mir-35* seed to recruit ZSWIM8/EBAX-1 or induce Argonaute conformational changes (Figure 4E). Because of the large number of possible trigger RNAs or trigger RBPs, further elucidating this mechanism will require large scale biochemical and genetic screens.

Understanding the seed sequence-specific decay mechanism regulating *mir-35* will have broad impact. Such seed-specific mechanisms are likely to be present in other biological systems because they allow for simultaneous regulation of redundant paralogs, enabling dynamic regulation of a miRNA seed family's targets. Outside functioning in normal physiology, seed-specific decay mechanisms could be an attractive avenue for modulating abundance of specific miRNA families and their target genes in disease.

Materials and Methods

General *C. elegans* culture and maintenance

C. elegans were maintained at 20°C on NGM seeded with OP50. For large-scale harvest of embryos, 8,000 starved L1s were plated onto a 10cm plate with a large lawn of OP50. The worms

were re-fed with concentrated OP50 48 hours later. At 96 hours after initial plating, the gravid adults were harvested by bleaching to collect large quantities of embryos.

Liquid culture

For experiments in which deep sequencing was performed (Figures 1 and 2), worms were grown
365 in liquid culture as previously described and harvested with some modifications (Zanin et al., 2011). Briefly, the gravid worms were harvested by centrifugation at 3000xg for 2 minutes in 50mL conical tubes. They were washed once with room temperature water and then pelleted. The volume of the sample was brought up to 28mL with water, and then 4mL of 5M NaOH and 8mL of 4% sodium hypochlorite were added. The tubes were immediately shaken vigorously for 2
370 minutes and allowed to rest on the bench for 1 minute, and this shaking and resting was repeated three times. The worms were immediately centrifuged at 3000xg for 2 minutes. The supernatant was decanted, and the worms were washed four times with 45mL of water. The synchronized embryos were either collected for the embryo samples, or M9 with cholesterol was added, and the worms were placed on a rocker at 20°C overnight to obtain a population of synchronized,
375 starved L1 worms.

CRISPR/Cas9-mediated genome editing

For all CRISPR experiments, pre-assembled Cas9 RNPs were injected into germlines along with short homology-directed repair templates with ~35-nt homology arms (Paix et al., 2014). For all CRISPR injections, one of the guide RNAs used targeted *dpy-10* as a visible marker to select
380 plates with efficient genome editing (Arribere et al., 2014). crRNAs and tracrRNA were ordered from IDT (Alt-R) or Dharmacon (Edit-R), and annealed at 10μM in duplex buffer by heating to 95°C for 5 minutes and then cooling to room temperature. Injection mixes contained 2-4μM Cas9, 4μM total of pre-annealed gRNAs (comprised of gRNAs targeting *dpy-10* and the site of interest), 0.8μM of the *dpy-10* donor oligonucleotide, and the homology directed donor at 40-100ng/μl
385 (Table S2).

Mutations to *mir-35* were made by two rounds of CRISPR. First, as previously described (Yang et al., 2020b), two gRNAs recognizing the protospacers TTTCCATTAGAACTATCACC and ATTGCTGGTTTCTTCCACAG were used to create a 50bp deletion at the *mir-35* locus. This allele is *mir-35(cdb2):*

390 GCTGGTTTCTTCCACAGT-50bp_del-CTTTTCCACTTGCTCCAC. The strain carrying *mir-35(cdb2)* was then injected with homology-directed repair donors, along with a gRNA

(GGAGCAAGTGGAAAAGACTG) recognizing a sequence which is created by the *mir-35(cdb2)* mutation.

Deep sequencing library preparation and data analysis

395 Library preparation was performed using the NEBNext Small RNA Library Prep Set for Illumina with modifications as previously described (Vieux et al., 2021). Briefly, size selection was performed only after reverse transcription, using 8% urea gels to purify ~65-75nt RT products. Prior to loading on the gel, each RT reaction was treated with 5000units of RNAse H (New England Biolabs) for 30 minutes at 37°C.

400 Sequence analysis was performed on the NIH High Performance Computing Cluster. The 3' adapter sequence was trimmed using Cutadapt 3.4 (Martin, 2011). The reads were mapped to a custom genome file which was comprised of *C. elegans* genome WS280 with an additional chromosome containing the sequences of the spike-in miRNAs and the mutant *mir-35* precursors with flanking genomic sequence. Mapping was performed using bowtie2 2.4.4 (Langmead et al.,
405 2009) with the following settings: --no-unal --end-to-end --sensitive. BAM files were sorted and indexed using samtools 1.13 (Danecek et al., 2021). Reads were assigned to miRNAs using htseq 0.13.5 (Anders et al., 2015) with the following settings: --mode union --nonunique fraction -a 0. The htseq analysis was performed using a gff file modified from mirGeneDB (Fromm et al., 2015) by replacing mirGeneDB IDs with miRbase IDs (Kozomara and Griffiths-Jones, 2014) and adding
410 the intervals corresponding to the spike-in miRNAs and the *mir-35* mutant miRNAs in the custom genome file. For analysis of tailing and trimming, the Tailor package (Chou et al., 2015) was used with the genome file described above and FASTA files derived from mirGeneDB, but with IDs replaced by miRbase IDs and sequences for spike-in miRNAs and the *mir-35* mutant miRNAs appended.

415 RNA isolation

Total RNA was isolated by resuspending the sample in the recommended volume of Trizol reagent (Life Technologies), followed by vortexing at room temperature for fifteen minutes, followed by preparation according to the Trizol manufacturer's instructions.

Taqman miRNA qPCR

420 For all miRNA qPCR, 5µl reverse transcription reactions were performed using the TaqMan MicroRNA Reverse Transcription kit (ThermoFisher). For all samples, 1.66µl of total RNA at 6ng/µl were used in the reverse transcription. RT reactions were diluted 1:4 and 1.33µl was used in a 5µl qPCR reaction prepared using Taqman miRNA probes with the Taqman Universal

Mastermix II with UNG (ThermoFisher). Reactions were run in triplicate on the Applied
425 Biosystems QuantStudio Pro 6.

Data Availability

All raw sequence data will be deposited in NCBI Sequence Read Archive.

Funding

This work was funded by the NIDDK Intramural Research Program (ZIA DK075147).

430 **Acknowledgments**

We thank WormBase, the NIDDK Genomics Core, the NCI Genomics Core, and NIH High Performance Computing. Strains are regularly received from the CGC, which is funded by NIH Office of Research Infrastructure Programs (P40 OD010440). Thank you to members of the McJunkin lab, Eric Miska, Kenneth Murfitt, Michael Lichten, Joana Vidigal, John Kim, and Leemor
435 Joshua-Tor for helpful discussions.

References

Alvarez-Saavedra, E., and Horvitz, H.R. (2010). Many families of C. elegans microRNAs are not essential for development or viability. Curr. Biol. *20*, 367–373.

Ameres, S.L., Horwich, M.D., Hung, J.-H., Xu, J., Ghildiyal, M., Weng, Z., and Zamore, P.D. (2010). Target RNA-directed trimming and tailing of small silencing RNAs. Science *328*, 1534–1539.

Anders, S., Pyl, P.T., and Huber, W. (2015). HTSeq—a Python framework to work with high-throughput sequencing data. Bioinformatics *31*, 166–169.

Arribere, J.A., Bell, R.T., Fu, B.X.H., Artiles, K.L., Hartman, P.S., and Fire, A.Z. (2014). Efficient marker-free recovery of custom genetic modifications with CRISPR/Cas9 in Caenorhabditis elegans. Genetics *198*, 837–846.

Baccarini, A., Chauhan, H., Gardner, T.J., Jayaprakash, A.D., Sachidanandam, R., and Brown, B.D. (2011). Kinetic analysis reveals the fate of a microRNA following target regulation in mammalian cells. Curr. Biol. *21*, 369–376.

Bail, S., Swerdel, M., Liu, H., Jiao, X., Goff, L.A., Hart, R.P., and Kiledjian, M. (2010). Differential regulation of microRNA stability. RNA *16*, 1032–1039.

Bernstein, E., Caudy, A.A., Hammond, S.M., and Hannon, G.J. (2001). Role for a bidentate ribonuclease in the initiation step of RNA interference. Nature *409*, 363–366.

Bitetti, A., Mallory, A.C., Golini, E., Carrieri, C., Carreño Gutiérrez, H., Perlas, E., Pérez-Rico, Y.A., Tocchini-Valentini, G.P., Enright, A.J., Norton, W.H.J., et al. (2018). MicroRNA degradation by a conserved target RNA regulates animal behavior. Nat. Struct. Mol. Biol. *25*, 244–251.

Boele, J., Persson, H., Shin, J.W., Ishizu, Y., Newie, I.S., Sokilde, R., Hawkins, S.M., Coarfa, C., Ikeda, K., Takayama, K. -i., et al. (2014). PAPD5-mediated 3' adenylation and subsequent degradation of miR-21 is disrupted in proliferative disease. Proc. Natl. Acad. Sci. *111*, 11467–11472.

Bossé, G.D., Rüegger, S., Ow, M.C., Vasquez-Rifo, A., Rondeau, E.L., Ambros, V.R., and Simard, M.J. (2013). The decapping scavenger enzyme DCS-1 controls microRNA levels in Caenorhabditis elegans. Mol. Cell *50*, 281–287.

Brancati, G. and Grosshans, H. (2018). An interplay of miRNA abundance and target site architecture determines miRNA activity and specificity. Nucleic Acids Res. *46*, 3259–3269

Brennecke, J., Stark, A., Russell, R.B., and Cohen, S.M. (2005). Principles of microRNA-target recognition. PLoS Biol. *3*, e85.

Broughton, J.P., Lovci, M.T., Huang, J.L., Yeo, G.W., and Pasquinelli, A.E. (2016). Pairing beyond the Seed Supports MicroRNA Targeting Specificity. Mol. Cell *64*, 320–333.

Cazalla, D., Yario, T., Steitz, J.A., and Steitz, J. (2010). Down-regulation of a host microRNA by a Herpesvirus saimiri noncoding RNA. Science *328*, 1563–1566.

Chatterjee, S., Grosshans, H., and Großhans, H. (2009). Active turnover modulates mature microRNA activity in Caenorhabditis elegans. Nature *461*, 546–549.

Chatterjee, S., Fasler, M., Büssing, I., and Grosshans, H. (2011). Target-mediated protection of

endogenous microRNAs in C. elegans. Dev. Cell *20*, 388–396.

Chou, M. Te, Han, B.W., Hsiao, C.P., Zamore, P.D., Weng, Z., and Hung, J.H. (2015). Tailor: a computational framework for detecting non-templated tailing of small silencing RNAs. Nucleic Acids Res. *43*.

Dallaire, A., Frédérick, P.-M., and Simard, M.J. (2018). Somatic and Germline MicroRNAs Form Distinct Silencing Complexes to Regulate Their Target mRNAs Differently. Dev. Cell *47*, 239-247.e4.

Danecek, P., Bonfield, J.K., Liddle, J., Marshall, J., Ohan, V., Pollard, M.O., Whitwham, A., Keane, T., McCarthy, S.A., Davies, R.M., et al. (2021). Twelve years of SAMtools and BCFtools. Gigascience *10*.

Denli, A.M., Tops, B.B.J., Plasterk, R.H. a, Ketting, R.F., and Hannon, G.J. (2004). Processing of primary microRNAs by the Microprocessor complex. Nature *432*, 231–235.

Dexheimer, P.J., and Cochella, L. (2020). MicroRNAs: From Mechanism to Organism. Front. Cell Dev. Biol. *8*, 409.

Dexheimer, P.J., Wang, J., and Cochella, L. (2020). Two microRNAs are sufficient for embryogenesis in C. elegans. BioRxiv 2020.06.28.176024.

Doll, M.A., Soltanmohammadi, N., and Schumacher, B. (2019). ALG-2/AGO-Dependent mir-35 Family Regulates DNA Damage-Induced Apoptosis Through MPK-1/ERK MAPK Signaling Downstream of the Core Apoptotic Machinery in Caenorhabditis elegans. Genetics *213*, 173–194.

Elbarbary, R.A., Miyoshi, K., Myers, J.R., Du, P., Ashton, J.M., Tian, B., and Maquat, L.E. (2017a). Tudor-SN-mediated endonucleolytic decay of human cell microRNAs promotes G1/S phase transition. Science *356*, 859–862.

Elbarbary, R.A., Miyoshi, K., Hedaya, O., Myers, J.R., and Maquat, L.E. (2017b). UPF1 helicase promotes TSN-mediated miRNA decay. Genes Dev. *31*, 1483–1493.

Fang, W., and Bartel, D.P. (2015). The Menu of Features that Define Primary MicroRNAs and Enable De Novo Design of MicroRNA Genes. Mol. Cell *60*, 131–145.

Fromm, B., Billipp, T., Peck, L.E., Johansen, M., Tarver, J.E., King, B.L., Newcomb, J.M., Sempere, L.F., Flatmark, K., Hovig, E., et al. (2015). A Uniform System for the Annotation of Vertebrate microRNA Genes and the Evolution of the Human microRNAome. Http://Dx.Doi.Org/10.1146/Annurev-Genet-120213-092023 *49*, 213–242.

Ghini, F., Rubolino, C., Climent, M., Simeone, I., Marzi, M.J., and Nicassio, F. (2018). Endogenous transcripts control miRNA levels and activity in mammalian cells by target-directed miRNA degradation. Nat. Commun. *9*, 3119.

Gregory, R.I., Yan, K.-P., Amuthan, G., Chendrimada, T., Doratotaj, B., Cooch, N., and Shiekhattar, R. (2004). The Microprocessor complex mediates the genesis of microRNAs. Nature *432*, 235–240.

Grishok, A., Pasquinelli, A.E., Conte, D., Li, N., Parrish, S., Ha, I., Baillie, D.L., Fire, A., Ruvkun, G., and Mello, C.C. (2001). Genes and mechanisms related to RNA interference regulate expression of the small temporal RNAs that control C. elegans developmental timing. Cell *106*, 23–34.

Grün, D., Kirchner, M., Thierfelder, N., Stoeckius, M., Selbach, M., and Rajewsky, N. (2014).

Conservation of mRNA and protein expression during development of C. elegans. Cell Rep. *6*, 565–577.

Han, J., Lee, Y., Yeom, K.-H., Kim, Y.-K., Jin, H., and Kim, V.N. (2004). The Drosha-DGCR8 complex in primary microRNA processing. Genes Dev. *18*, 3016–3027.

Han, J., Lee, Y., Yeom, K.-H., Nam, J.-W., Heo, I., Rhee, J.-K., Sohn, S.Y., Cho, Y., Zhang, B.-T., and Kim, V.N. (2006). Molecular basis for the recognition of primary microRNAs by the Drosha-DGCR8 complex. Cell *125*, 887–901.

Han, J., LaVigne, C.A., Jones, B.T., Zhang, H., Gillett, F., and Mendell, J.T. (2020). A ubiquitin ligase mediates target-directed microRNA decay independently of tailing and trimming. Science *370*, eabc9546.

Helwak, A., Kudla, G., Dudnakova, T., and Tollervey, D. (2013). Mapping the Human miRNA Interactome by CLASH Reveals Frequent Noncanonical Binding. Cell *153*, 654.

Hutvágner, G., McLachlan, J., Pasquinelli, A.E., Bálint, E., Tuschl, T., and Zamore, P.D. (2001). A cellular function for the RNA-interference enzyme Dicer in the maturation of the let-7 small temporal RNA. Science *293*, 834–838.

Iwasaki, S., Kobayashi, M., Yoda, M., Sakaguchi, Y., Katsuma, S., Suzuki, T., and Tomari, Y. (2010). Hsc70/Hsp90 chaperone machinery mediates ATP-dependent RISC loading of small RNA duplexes. Mol. Cell *39*, 292–299.

Iwasaki, S., Sasaki, H.M., Sakaguchi, Y., Suzuki, T., Tadakuma, H., and Tomari, Y. (2015). Defining fundamental steps in the assembly of the Drosophila RNAi enzyme complex. Nature *521*, 533–536.

Kagias, K., and Pocock, R. (2015). microRNA regulation of the embryonic hypoxic response in Caenorhabditis elegans. Sci. Rep. *5*, 11284.

Kato, M., de Lencastre, A., Pincus, Z., and Slack, F.J. (2009). Dynamic expression of small non-coding RNAs, including novel microRNAs and piRNAs/21U-RNAs, during Caenorhabditis elegans development. Genome Biol. *10*, R54.

Katoh, T., Hojo, H., and Suzuki, T. (2015). Destabilization of microRNAs in human cells by 3′ deadenylation mediated by PARN and CUGBP1. Nucleic Acids Res. *43*, 7521–7534.

Ketting, R.F., Fischer, S.E., Bernstein, E., Sijen, T., Hannon, G.J., and Plasterk, R.H. (2001). Dicer functions in RNA interference and in synthesis of small RNA involved in developmental timing in C. elegans. Genes Dev. *15*, 2654–2659.

Kingston, E.R., and Bartel, D.P. (2019). Global analyses of the dynamics of mammalian microRNA metabolism. Genome Res. *29*, 1777–1790.

Kleaveland, B., Shi, C.Y., Stefano, J., and Bartel, D.P. (2018). A Network of Noncoding Regulatory RNAs Acts in the Mammalian Brain. Cell *174*, 350-362.e17.

Knight, S.W., and Bass, B.L. (2001). A role for the RNase III enzyme DCR-1 in RNA interference and germ line development in Caenorhabditis elegans. Science *293*, 2269–2271.

Knouf, E.C., Wyman, S.K., and Tewari, M. (2013). The human TUT1 nucleotidyl transferase as a global regulator of microRNA abundance. PLoS One *8*, e69630.

Kozomara, A., and Griffiths-Jones, S. (2014). MiRBase: Annotating high confidence microRNAs using deep sequencing data. Nucleic Acids Res. *42*, D68–D73.

560 Krol, J., Busskamp, V., Markiewicz, I., Stadler, M.B., Ribi, S., Richter, J., Duebel, J., Bicker, S., Fehling, H.J., Schübeler, D., et al. (2010). Characterizing light-regulated retinal microRNAs reveals rapid turnover as a common property of neuronal microRNAs. Cell *141*, 618–631.

Landthaler, M., Yalcin, A., and Tuschl, T. (2004). The Human DiGeorge Syndrome Critical Region Gene 8 and Its D. melanogaster Homolog Are Required for miRNA Biogenesis. Curr.
565 Biol. *14*, 2162–2167.

Langmead, B., Trapnell, C., Pop, M., and Salzberg, S.L. (2009). Ultrafast and memory-efficient alignment of short DNA sequences to the human genome. Genome Biol. *10*, R25.

Lee, D., Park, D., Park, J.H., Kim, J.H., and Shin, C. (2019). Poly(A)-specific ribonuclease sculpts the 3′ ends of microRNAs. RNA *25*, 388–405.

570 Lee, M., Choi, Y., Kim, K., Jin, H., Lim, J., Nguyen, T.A.A., Yang, J., Jeong, M., Giraldez, A.J.J., Yang, H., et al. (2014). Adenylation of maternally inherited microRNAs by Wispy. Mol. Cell *56*, 696–707.

Lehrbach, N.J., Castro, C., Murfitt, K.J., Abreu-Goodger, C., Griffin, J.L., and Miska, E.A. (2012). Post-developmental microRNA expression is required for normal physiology, and
575 regulates aging in parallel to insulin/IGF-1 signaling in C. elegans. RNA *18*, 2220–2235.

Lewis, B.P., Shih, I., Jones-Rhoades, M.W., Bartel, D.P., and Burge, C.B. (2003). Prediction of mammalian microRNA targets. Cell *115*, 787–798.

Libri, V., Helwak, A., Miesen, P., Santhakumar, D., Borger, J.G., Kudla, G., Grey, F., Tollervey, D., and Buck, A.H. (2012). Murine cytomegalovirus encodes a miR-27 inhibitor disguised as a
580 target. Proc. Natl. Acad. Sci. U. S. A. *109*, 279–284.

Liu, M., Liu, P., Zhang, L., Cai, Q., Gao, G., Zhang, W., Zhu, Z., Liu, D., and Fan, Q. (2011). mir-35 is involved in intestine cell G1/S transition and germ cell proliferation in C. elegans. Cell Res. *21*, 1605–1618.

Ma, H., Wu, Y., Choi, J.-G., and Wu, H. (2013). Lower and upper stem-single-stranded RNA
585 junctions together determine the Drosha cleavage site. Proc. Natl. Acad. Sci. U. S. A. *110*, 20687–20692.

Marcinowski, L., Tanguy, M., Krmpotic, A., Rädle, B., Lisnić, V.J., Tuddenham, L., Chane-Woon-Ming, B., Ruzsics, Z., Erhard, F., Benkartek, C., et al. (2012). Degradation of cellular mir-27 by a novel, highly abundant viral transcript is important for efficient virus replication in vivo.
590 PLoS Pathog. *8*, e1002510.

Martin, M. (2011). Cutadapt removes adapter sequences from high-throughput sequencing reads. EMBnet.Journal *17*, 10–12.

Marzi, M.J., Ghini, F., Cerruti, B., De Pretis, S., Bonetti, P., Giacomelli, C., Gorski, M.M., Kress, T., Pelizzola, M., Muller, H., et al. (2016). Degradation dynamics of micrornas revealed by a
595 novel pulse-chase approach. Genome Res. *26*, 554–565.

Massirer, K.B., Perez, S.G., Mondol, V., and Pasquinelli, A.E. (2012). The miR-35-41 family of microRNAs regulates RNAi sensitivity in Caenorhabditis elegans. PLoS Genet. *8*, e1002536.

la Mata, M., Gaidatzis, D., Vitanescu, M., Stadler, M.B., Wentzel, C., Scheiffele, P., Filipowicz, W., and Großhans, H. (2015). Potent degradation of neuronal mi RNA s induced by highly
600 complementary targets . EMBO Rep. *16*, 500–511.

McJunkin, K., and Ambros, V. (2014). The embryonic mir-35 family of microRNAs promotes

multiple aspects of fecundity in Caenorhabditis elegans. G3 (Bethesda). *4*, 1747–1754.

McJunkin, K., and Ambros, V. (2017). A microRNA family exerts maternal control on sex determination in C. elegans. Genes Dev. *31*, 422–437.

Miki, T.S., Rüegger, S., Gaidatzis, D., Stadler, M.B., and Großhans, H. (2014). Engineering of a conditional allele reveals multiple roles of XRN2 in Caenorhabditis elegans development and substrate specificity in microRNA turnover. Nucleic Acids Res. *42*, 4056–4067.

Paix, A., Wang, Y., Smith, H.E., Lee, C.Y.S., Calidas, D., Lu, T., Smith, J., Schmidt, H., Krause, M.W., and Seydoux, G. (2014). Scalable and versatile genome editing using linear DNAs with microhomology to Cas9 sites in Caenorhabditis elegans. Genetics *198*, 1347–1356.

Parchem, R.J., Moore, N., Fish, J.L., Parchem, J.G., Braga, T.T., Shenoy, A., Oldham, M.C., Rubenstein, J.L.R., Schneider, R.A., and Blelloch, R. (2015). miR-302 Is Required for Timing of Neural Differentiation, Neural Tube Closure, and Embryonic Viability. Cell Rep. *12*, 760–773.

Piwecka, M., Glažar, P., Hernandez-Miranda, L.R., Memczak, S., Wolf, S.A., Rybak-Wolf, A., Filipchyk, A., Klironomos, F., Cerda Jara, C.A., Fenske, P., et al. (2017). Loss of a mammalian circular RNA locus causes miRNA deregulation and affects brain function. Science *357*, eaam8526.

Reichholf, B., Herzog, V.A., Fasching, N., Manzenreither, R.A., Sowemimo, I., and Ameres, S.L. (2019). Time-Resolved Small RNA Sequencing Unravels the Molecular Principles of MicroRNA Homeostasis. Mol. Cell *75*, 756-768.e7.

Rissland, O.S., Hong, S.-J., and Bartel, D.P. (2011). MicroRNA destabilization enables dynamic regulation of the miR-16 family in response to cell-cycle changes. Mol. Cell *43*, 993–1004.

Sherrard, R., Luehr, S., Holzkamp, H., McJunkin, K., Memar, N., and Conradt, B. (2017). Mirnas cooperate in apoptosis regulation during c. Elegans development. Genes Dev. *31*, 209–222.

Sheu-Gruttadauria, J., Pawlica, P., Klum, S.M., Wang, S., Yario, T.A., Schirle Oakdale, N.T., Steitz, J.A., and MacRae, I.J. (2019). Structural Basis for Target-Directed MicroRNA Degradation. Mol. Cell *75*, 1243-1255.e7.

Shi, C.Y., Kingston, E.R., Kleaveland, B., Lin, D.H., Stubna, M.W., and Bartel, D.P. (2020). The ZSWIM8 ubiquitin ligase mediates target-directed microRNA degradation. Science *370*, eabc9359.

Shukla, S., Bjerke, G.A., Muhlrad, D., Yi, R., and Parker, R. (2019). The RNase PARN Controls the Levels of Specific miRNAs that Contribute to p53 Regulation. Mol. Cell *73*, 1204-1216.e4.

Stoeckius, M., Maaskola, J., Colombo, T., Rahn, H.-P., Friedländer, M.R., Li, N., Chen, W., Piano, F., and Rajewsky, N. (2009). Large-scale sorting of C. elegans embryos reveals the dynamics of small RNA expression. Nat. Methods *6*, 745–751.

Tran, A.T., Chapman, E.M., Flamand, M.N., Yu, B., Krempel, S.J., Duchaine, T.F., Eroglu, M., and Derry, W.B. (2019). MiR-35 buffers apoptosis thresholds in the C. elegans germline by antagonizing both MAPK and core apoptosis pathways. Cell Death Differ. *26*, 2637–2651.

Vieux, K.-F., Prothro, K.P., Kelley, L.H., Palmer, C., Maine, E.M., Veksler-Lublinsky, I., and McJunkin, K. (2021). Screening by deep sequencing reveals mediators of microRNA tailing in C. elegans. Nucleic Acids Res. *49*, 11167–11180.

Wang, Z., Hou, Y., Guo, X., vanderVoet, M., Boxem, M., Dixon, J.E., Chisholm, A.D., and Jin, Y. (2013). The EBAX-type Cullin-RING E3 Ligase and Hsp90 Guard the Protein Quality of the

SAX-3/Robo Receptor in Developing Neurons. Neuron *79*, 903–916.

645 Wu, E., Thivierge, C., Flamand, M., Mathonnet, G., Vashisht, A.A., Wohlschlegel, J., Fabian, M.R., Sonenberg, N., and Duchaine, T.F. (2010). Pervasive and cooperative deadenylation of 3'UTRs by embryonic microRNA families. Mol. Cell *40*, 558–570.

Wyman, S.K., Knouf, E.C., Parkin, R.K., Fritz, B.R., Lin, D.W., Dennis, L.M., Krouse, M.A., Webster, P.J., and Tewari, M. (2011). Post-transcriptional generation of miRNA variants by
650 multiple nucleotidyl transferases contributes to miRNA transcriptome complexity. Genome Res. *21*, 1450–1461.

Yang, A., Shao, T.-J., Bofill-De Ros, X., Lian, C., Villanueva, P., Dai, L., and Gu, S. (2020a). AGO-bound mature miRNAs are oligouridylated by TUTs and subsequently degraded by DIS3L2. Nat. Commun. *11*, 2765.

655 Yang, B., Schwartz, M., and McJunkin, K. (2020b). In vivo CRISPR screening for phenotypic targets of the mir-35-42 family in C. elegans. Genes Dev. *34*, 1227–1238.

Ye Duan, Isana Veksler-Lublinsky, V.A. (2021). Critical contribution of 3' non-seed base pairing to the in vivo function of the evolutionarily conserved let-7a microRNA. Biorxiv.

Zanin, E., Dumont, J., Gassmann, R., Cheeseman, I., Maddox, P., Bahmanyar, S., Carvalho, A.,
660 Niessen, S., Yates, J.R., Oegema, K., et al. (2011). Affinity purification of protein complexes in C. elegans. Methods Cell Biol. *106*, 289–322.

Zeng, Y., Yi, R., and Cullen, B.R. (2005). Recognition and cleavage of primary microRNA precursors by the nuclear processing enzyme Drosha. EMBO J. *24*, 138–148.

Zhao, Y., Jin, L., Wang, Y., Kong, Y., and Wang, D. (2019). Prolonged exposure to multi-walled
665 carbon nanotubes dysregulates intestinal mir-35 and its direct target MAB-3 in nematode Caenorhabditis elegans. Sci. Rep. *9*.

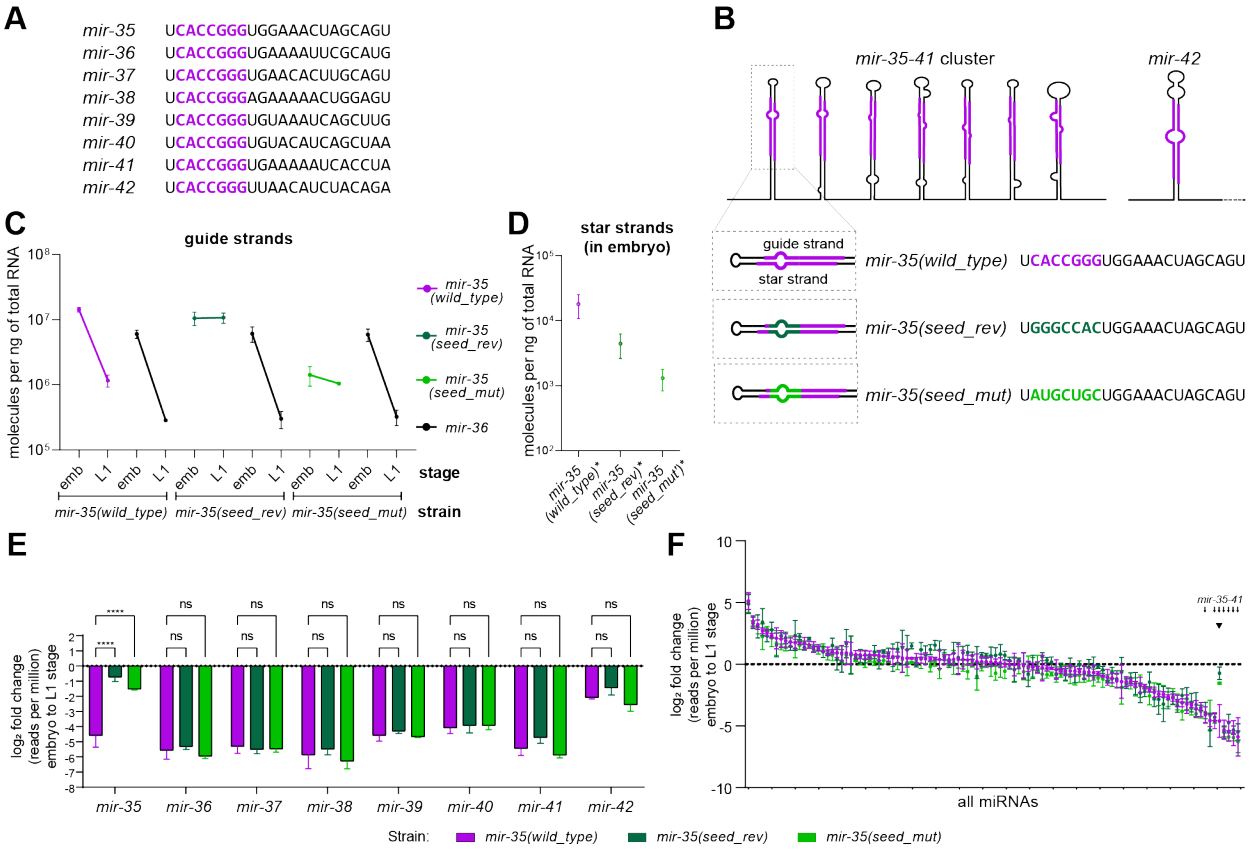

670 **Figure 1. *mir-35* decay is seed sequence-dependent** (A) Sequences of *mirs-35-42*. The identical seed sequence is shown in purple. (B) Schematic of the *mir-35-41* cluster and *mir-42* showing the structure of the hairpins in the primary transcripts. The guide and star strands are highlighted in purple (top). Below is the wild type *mir-35* sequence (purple) and the two seed mutant *mir-35* variants (green). Both seed mutant *mir-35* variants have compensatory mutations
675 to the star strand to maintain the wild type-like structure of the mutant *mir-35* hairpin. (C) Absolute quantification of *mir-35* and *mir-36* in embryos and L1. For some error bars, the range is smaller than the symbol. (D) Absolute quantification of star strands of *mir-35* and mutant variants in embryos. (E-F) Log_2(fold change) in abundance from embryo to L1, calculated from normalized deep sequencing reads for either the *mir-35-42* family (E) or all miRNAs with >50 RPM in wild
680 type (F). Note that color of bar indicates strain, not necessarily a mutant miRNA; only *mir-35* is mutated in the indicated mutant strains. (E) Two-way ANOVA was performed, followed by Dunnett's multiple comparisons test. ****p-value < 0.0001 Small arrows in (F) indicate positions of *mir-35-41* on ranked x-axis, and arrowhead indicates *mir-35* with mutant variants. (C-F) Mean and SEM of three biological replicates are shown.

685

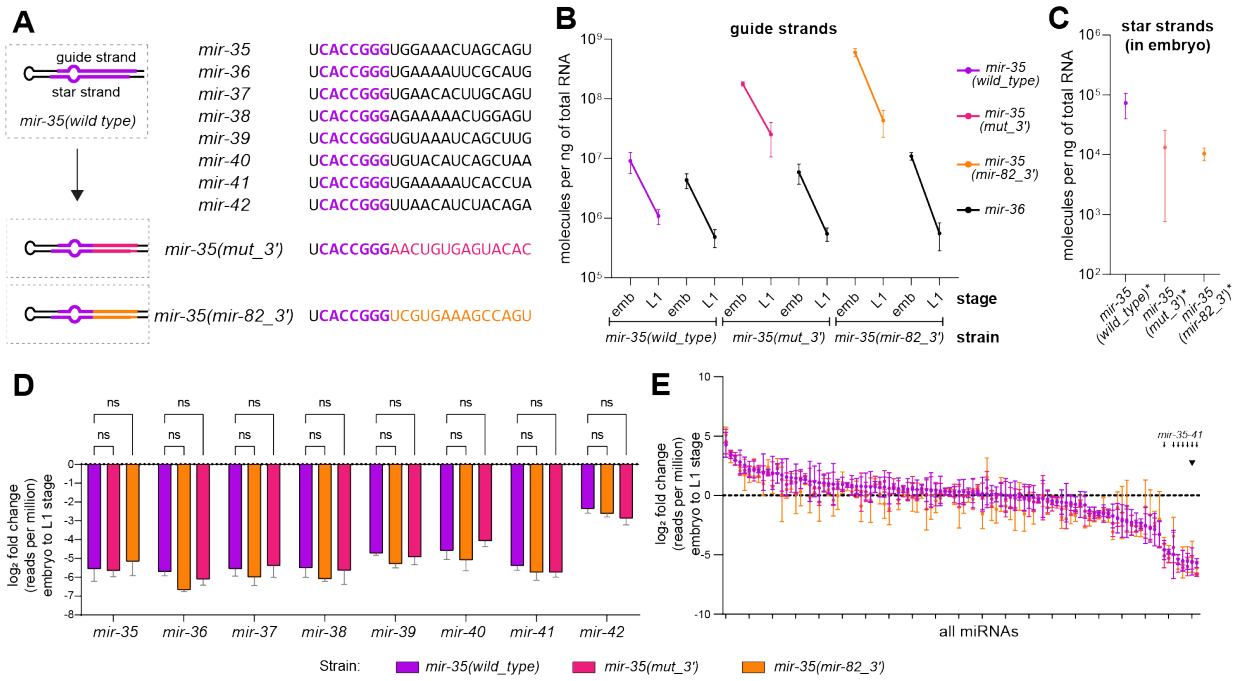

Figure 2. *mir-35* 3' end mutants do not alter decay (A) Sequences of *mirs-35-42* with the identical seed sequences shown in purple (top). Schematic of the *mir-35* 3' end mutants (bottom). Both 3' end mutants have compensatory mutations to the star strand to maintain the wild type like structure of the mutant *mir-35* hairpin. (B) Absolute quantification of *mir-35* and *mir-36* in embryos and L1. Mean and SEM of two to three biological replicates are shown. (C) Absolute quantification of star strands of *mir-35* and mutant variants in embryos. (D-E) Log_2(fold change) in abundance from embryo to L1, calculated from normalized deep sequencing reads for either the *mir-35-42* family (D) or all miRNAs with >50 RPM in wild type (E). Note that color of bar indicates strain, not necessarily a mutant miRNA; only *mir-35* is mutated in the indicated mutant strains. (D) Two-way ANOVA was performed, followed by Dunnett's multiple comparisons test. Small arrows in (E) indicate positions of *mir-35-41* on ranked x-axis, and arrowhead indicates *mir-35* with mutant variants. (C-E) Mean and SEM of three biological replicates are shown.

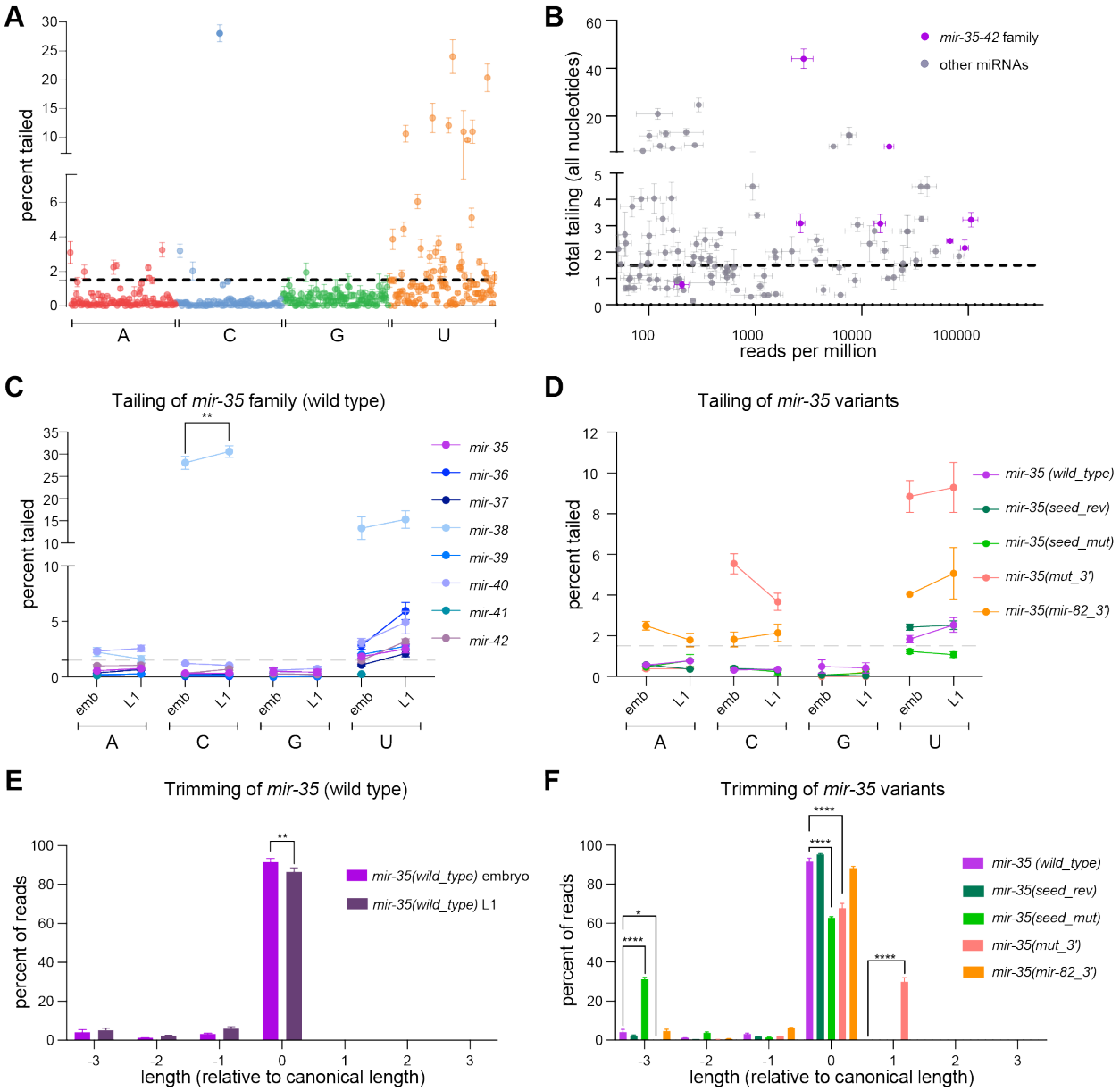

Figure 3. Changes in tailing and trimming of *mir-35* variants do not correlate with changes in decay (A) Percent of reads with single nucleotide addition to the 3' end is shown for each miRNA with >50 RPM in embryo. (B) Total tailing (sum of all single nucleotide tails) versus abundance (RPM) is shown for all miRNAs with >50 RPM in embryo. The *mir-35* family is highlighted in purple. (C-D) Percent of reads with single nucleotide additions to the *mir-35* family (C) and the *mir-35* variants (D) in the embryo and L1. (E-F) Percent of reads of each length (excluding tail), relative to the canonical length of *mir-35* in wild type embryo and L1 (E) or *mir-35* variants in embryo (F). (A-F) Mean and SEM are shown for six biological replicates for wild type and three biological replicates for all *mir-35* variant strains. (C-F) For each nucleotide, one-way ANOVA was performed, followed by Sidak's multiple comparison test. Significant relationships in panel D are described in the text, but not indicated on the graph for simplicity. *p-value < 0.05, **p-value < 0.01, ****p-value < 0.0001.

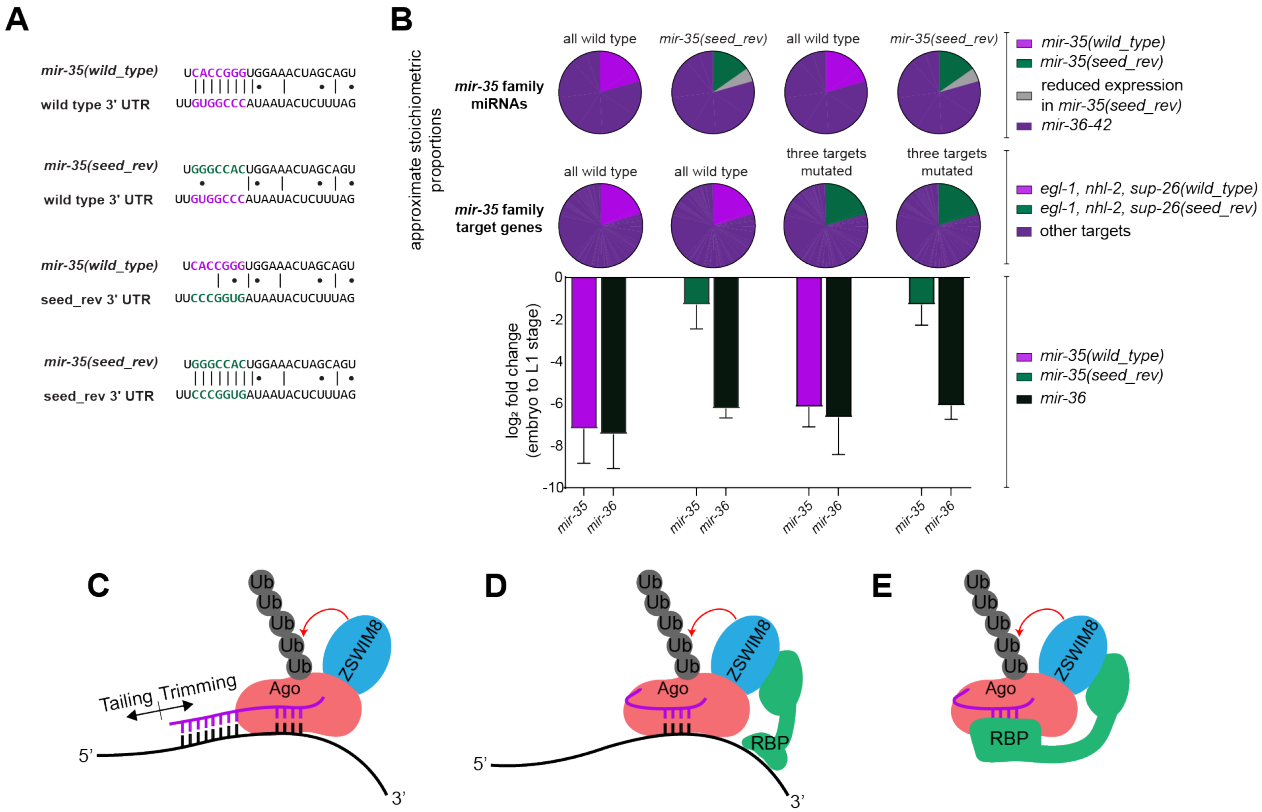

Figure 4. Reintroducing miRNA-target interactions does not restore decay of a seed mutant variant of *mir-35* (A) Target binding sites for *mir-35(seed_rev)* were introduced to the 3'UTR of three known *mir-35* targets (*egl-1, sup-26* and *nhl-2*), either in a *mir-35(wild_type)* or a *mir-35(seed_rev)* background. An example of the relevant miRNA-target interactions at the *egl-1* 3'UTR are shown. (B) Top: Pie charts represent an estimate of the proportion of the *mir-35* family molecules and the *mir-35* family target molecules that are mutated in each strain. Bottom: Log_2(fold change) from embryo to L1 in the indicated strains, as measured by Taqman qPCR. Mean and SEM of three biological replicates are shown. (C) Model of conventional TDMD. (D-E) Alternative models for regulation of *mir-35* family decay, in which the seed sequence is recognized by a complementary RNA (D) or an RNA-binding protein (RBP) (E).